High Resolution Optical Frequency Domain Reflectometry for Analyzing Intra-Chip Reflections

Dan Zhao, Dzmitry Pustakhod, Kevin Williams, and Xaveer Leijtens

***Abstract*— We present a method for high-resolution optical frequency domain reflectometry by de-embedding group-velocity dispersion in the device under test. The method is shown to provide an accurate estimation of the wavelength-dependent group refractive index, and provides a spatial resolution of $5.3 \pm 1.7\,\mu$m for intra-chip reflections. We applied this method to characterize localized reflections from a number of waveguide crossings. The minimum distance of 30 μm between two crossings could easily be resolved. The reflection of waveguide crossings was analyzed to be $(2.5 \pm 1.2) \cdot 10^{-6}$.**

***Index Terms*— OFDR, photonic integrated circuits, reflection coefficient, spatial resolution.**

I. Introduction

IN PHOTONIC integrated circuits (PICs), intra-chip reflections from waveguide defects and mode-mismatching can lead to interference with signals both on and off chip [1], [2]. They result in an unwanted change of the behavior of circuits, especially for circuits containing active components. The influence becomes stronger as the complexity of circuits increases. So it is essential to characterize the localized reflections of components in order to take the effects into account during circuit design and to improve component design. The optical reflectometry methods have been well developed for characterization of localized reflections in fiber optics [3]–[5]. However, there are challenges for characterization of PICs, such as the higher requirements of the spatial resolution [6]. The feature size of components in PICs is as low as micrometers and they are closely spaced. With the stronger demands of reducing footprint of PICs, the improvement of spatial resolution of the optical reflectometry methods is becoming increasingly significant.

There are three main optical reflectometry methods: optical time domain reflectometry (OTDR), optical coherence domain reflectometry (OCDR) and optical frequency domain reflectometry (OFDR). They have tradeoffs in spatial resolution, sensitivity and length range [4], [7], [8]. Recently, the OFDR method has drawn more attentions due to its high speed and sensitivity, compact setup, and easy adjustment of the spatial resolution [9], [10]. However, the spatial resolution of OFDR is typically limited to tens of micrometers [6], [8]. Iizuka et al. have reported a 5.4 μm spatial resolution obtained with OFDR, but with low-dispersion waveguides over a 500 µm distance [11]. The deterioration of the spatial resolution due to dispersion in their case is negligible. In this work, we have achieved a comparable spatial resolution of $5.3 \pm 1.7\,\mu$m with OFDR for more dispersive waveguides over a longer spatial range. There are two key factors which result in the high resolution: first, the use of a coherent tunable laser source with a broad tuning range; second, the correction for the error incurred by an unknown waveguide dispersion. Glombitza et al. have established a method for dispersion correction in OFDR. They have achieved a spatial resolution of 50 μm, limited by the laser tuning range [6]. Compared to their method, the novelties of our work are: first, we have a simplified system with higher stability; second, we provide an accurate method for estimating the wavelength dependent group and effective refractive index of dispersive waveguides.

Lastly, we have experimentally investigated the OFDR method with the characterization of shallow ridge waveguide crossings on InP. Such waveguide crossings play an important role in PICs. However, they cause localized reflections [12]. We used samples with waveguide crossings to experimentally confirm the spatial resolution of our method and in addition, to characterize the reflection of ridge waveguide crossings on InP.

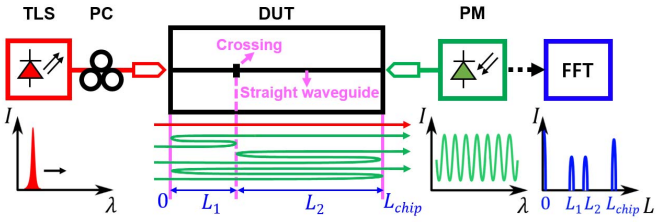

Fig. 1. A schematic diagram of the OFDR system.

II. The OFDR Method

A schematic diagram of the OFDR system is shown in Fig. 1. Light from a swept tunable laser source (TLS) is aligned to the TE-polarized mode of the PIC waveguide through a polarization controller (PC). It is coupled into the device under test (DUT) with a lensed fiber. The DUT contains shallow-etched straight waveguides on InP [12] and the crossings, short waveguide intersections at a 90° angle. The intensity modulation resulting from the interference between the direct signal (red path), acting as a reference, and the signals with multiple reflections between the cleaved facets

Manuscript received April 10, 2017; revised June 2, 2017; accepted June 27, 2017. Date of publication July 4, 2017; date of current version July 21, 2017. This work was supported in part by the Memphis Project 13538 and in part by the Dutch Technology Foundation STW. This paper was presented at the 18th European Conference on Integrated Optics, Warsaw, Poland, May 2016. *(Corresponding author: Dan Zhao.)*

The authors are with the COBRA Research Institute, Eindhoven University of Technology, 5612 AJ Eindhoven, The Netherlands (e-mail: d.zhao@tue.nl).

Color versions of one or more of the figures in this letter are available online at http://ieeexplore.ieee.org.

Digital Object Identifier 10.1109/LPT.2017.2723242

1041-1135 © 2017 IEEE. Translations and content mining are permitted for academic research only. Personal use is also permitted, but republication/redistribution requires IEEE permission. See http://www.ieee.org/publications_standards/publications/rights/index.html for more information.

and the waveguide crossing (green paths) is recorded by the power meter (PM) when sweeping the TLS. Taking the Fast Fourier transform (FFT) of the output signal, a map of the distribution of all reflections in the spatial domain can be retrieved, shown schematically as the blue curve in Fig. 1 [13], [14]. It is then possible to determine the position and the reflection of the crossing. It is worth noting that one crossing results in two reflection peaks due to the two interference paths that exist between the crossing and the front and back facets, respectively. Since the sample itself provides the interferometers, in contrast to a prior OFDR concept [6], there is no need for external mirrors which leads to a compact system and an enhanced measurement stability.

The frequency or wavelength span used in the measurements determines the spatial resolution of the OFDR method in a waveguide without group velocity dispersion (ideal case), according to eq. (1) [4]

$$\delta L = \frac{c}{2n_{\mathrm{g}}\Delta f} \tag{1}$$

where c is the speed of light in vacuum, n_{g} is the group index of the waveguide and Δf is the frequency span. A broad wavelength span of 100 nm results in a high spatial resolution of about 3 μm. However, the integrated waveguides are dispersive. It results in a loss in spatial resolution, demonstrated by Glombitza and Brinkmeyer [6]. A product of the group index change over the broad wavelength span and the distance from the input end of the waveguide to the particular reflector under consideration determines the deterioration factor of the spatial resolution. Therefore, it is important to de-embed group velocity dispersion to achieve a spatial resolution comparable to the theoretical limit, especially for a long spatial range.

In the ideal case, the group refractive index is constant and the effective refractive index depends linearly on the wavelength. In the real case, the effective refractive index contains higher order terms due to dispersion. We take a second order approximation of the effective refractive index $n_{\mathrm{eff}}(\lambda) \approx n_{\mathrm{eff}}(\lambda_0) + n'_{\mathrm{eff}}(\lambda_0)(\lambda - \lambda_0) + \frac{1}{2}n''_{\mathrm{eff}}(\lambda_0)(\lambda - \lambda_0)^2$, where in our case λ_0 is 1550 nm, $n_{\mathrm{eff}}(\lambda_0) \approx 3.23$, $n_{\mathrm{g}}(\lambda_0)$, $n'_{\mathrm{eff}}(\lambda_0) = (n_{\mathrm{eff}}(\lambda_0) - n_{\mathrm{g}}(\lambda_0))/\lambda_0$ and $n''_{\mathrm{eff}}(\lambda_0)$ are to be determined [6], [7]. The de-embedding of dispersion in the spatial domain can be realized by rescaling the optical wavelength $\lambda/n_{\mathrm{eff}}(\lambda)$ at each recorded power before applying the FFT.

We provide a numerical algorithm to extract the quadratic term of $n_{\mathrm{eff}}(\lambda)$ from the recorded power spectrum: first, instead of taking the FFT of the whole spectrum, we apply the FFT to a small portion. It is selected by a rectangular window $[\lambda - \Delta w/2, \lambda + \Delta w/2]$, where Δw is the window width. The FFT is performed after translating the spectral interferogram to equally-spaced optical frequencies. This allows the extraction of the temporal trace at wavelength λ. The temporal axis is scaled according to eq. (2).

$$\tau(i) = \frac{1}{2}\delta\tau\frac{i}{N} \tag{2}$$

where i is the sample index, N is the total number of inputs, $\delta\tau$ is the group delay interval, it is inversely proportional to the frequency interval. Moving the rectangular window over the whole spectrum will yield the temporal traces versus wavelength. Second, extract the group index of the dispersive waveguide according to eq. (3) [4], [15].

$$n_{\mathrm{g}}(\lambda) = c\frac{\tau_{\mathrm{b}}(\lambda) - \tau_{\mathrm{f}}(\lambda)}{L_{\mathrm{chip}}} \tag{3}$$

where τ_{f} and τ_{b} are the group delays of front and back facet reflections, which are retrieved from the first step, and L_{chip} is the length of the integrated chip. The accuracy of the group index is in the order of 10^{-2}, which is determined by the measurement accuracy of the chip length $\delta n_{\mathrm{g}} = \frac{\delta L_{\mathrm{chip}}}{L_{\mathrm{chip}}} n_{\mathrm{g}}$ ($L_{\mathrm{chip}} = 4600\,\mu$m, $\delta L_{\mathrm{chip}} \approx 15\,\mu$m, $n_{\mathrm{g}} \approx 3.67$) [13]. Third, extract the quadratic term of $n_{\mathrm{eff}}(\lambda)$ from the extracted $n_{\mathrm{g}}(\lambda)$ according to eq. (4) and (5) [16], [17].

$$n_{\mathrm{g}}(\lambda) \approx a - b\lambda_0 - c\lambda_0(\lambda - \lambda_0) \tag{4}$$

$$n_{\mathrm{eff}}(\lambda) \approx a + b(\lambda - \lambda_0) + \frac{1}{2}c(\lambda - \lambda_0)^2 \tag{5}$$

where $a = n_{\mathrm{eff}}(\lambda_0), b = n'_{\mathrm{eff}}(\lambda_0), c = n''_{\mathrm{eff}}(\lambda_0)$. Fourth, perform the FFT to the modified spectrum $P(\lambda/n_{\mathrm{eff}}(\lambda))$ with a rectangular window. This will finally remove the dispersion-induced limitations to both the spatial resolution and the amplitude accuracy. Different window functions can be used to find tradeoffs of spatial resolution, peak accuracy, and suppression of side-lobes [18]. Based on this numerical algorithm, the dispersion of different DUT can be de-embedded accurately by extracting the $n_{\mathrm{eff}}(\lambda)$ for each case. There is no need of extra measurements for de-embedding dispersion, so the system realizes a self-calibration of the spatial resolution.

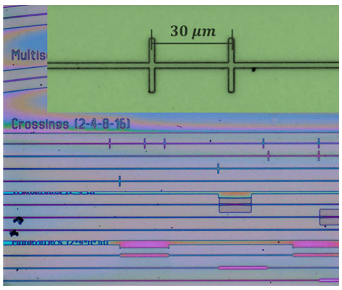

Fig. 2. Microscope photograph of a small section of the integrated chip under test. The inset shows a photograph of two crossings with a distance of 30 μm.

III. Characterization of Waveguide Crossings

A. Device Under Test

The OFDR system is experimentally investigated with the DUT fabricated by Smart Photonics through the JePPIX.eu multi-project wafer (MPW) service [19]. A microscope photograph of a small section of the integrated chip is shown in Fig. 2. There are several shallow-etched waveguides which contain a different number of crossings. The width of waveguides is 2 μm. To analyze variability of measurement data, devices from three MPW runs have been characterized. OFDR measurements for a waveguide with 8 crossings at distances 1170, 1200, 2250, 2350, 2470, 3400, 3850 and 3950 μm from the front facet, respectively, are presented in the

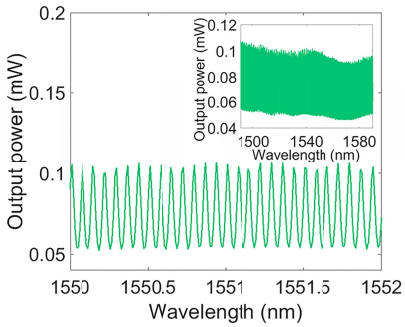

Fig. 3. The interference fringes of transmitted light. The inset shows the transmission spectrum in a broad wavelength range of the DUT.

next section. The smallest separation between two crossings is 30 μm as is shown in the inset of Fig. 2.

B. The OFDR Characterization

A wavelength span of 100 nm with a step of 0.01 nm of the TLS (Agilent 81600B) is used in our measurements. The interference fringes of the transmitted light are recorded by a PM (Agilent 81636B) as shown in Fig. 3. The fringe interval corresponds to a cavity length of 4600 μm formed by the two facets of the chip. The transmission spectrum of the DUT in a broad wavelength range of 1490 nm to 1590 nm is shown in the inset of Fig. 3. The depth of the modulation in the spectrum is quite uniform over the whole wavelength range. There are slight additional modulations due to beating between the fundamental and higher-order modes. The excitation of higher-order modes is caused by imperfect alignment.

A data processing is done by following the numerical algorithm discussed above. We use a moving rectangular window with a width of 20 nm. It is chosen to make a tradeoff between the resolution of the temporal trace and the accuracy of the approximated group refractive index at wavelength λ. To extract only the linear tendency for the group delay, such a wide window is sufficient. The moving step of the window is 0.2 nm. The group refractive index of the waveguide $n_g(\lambda)$ is extracted, shown as the blue line in Fig. 4(a). It is linearly fitted (magenta line) to find the solution of the coefficients in eq. (4) and (5) [20]. Then we apply the FFT to the power spectrum before and after de-embedding dispersion. The distributions of the intra-chip reflections as a function of the cavity length in the two cases are shown in Fig. 4(b) and (c), respectively. The reflections are normalized to the maximum intensity.

As shown in Fig. 4(b), the reflections caused by the facets and the crossings are detected. However, an increasing broadening of the reflection peaks occurs with increasing cavity length, which results in an underestimation of reflections. This can be verified by calculating the relative intensity RI at the cavity length of L_{chip}. It is only determined by the facet reflection and the propagation loss based on the condition that the crossing reflections are much lower than those from the facets, $|r_c|^2 \ll |r_f|^2$, which is the case here [7], [21]:

$$RI \approx |r_f|^2 e^{-\alpha L_{\text{chip}}} \tag{6}$$

where the reflection coefficient r_f of cleaved facet is $\sqrt{0.33 \pm 0.03}$ [22], the propagation loss α is measured to be

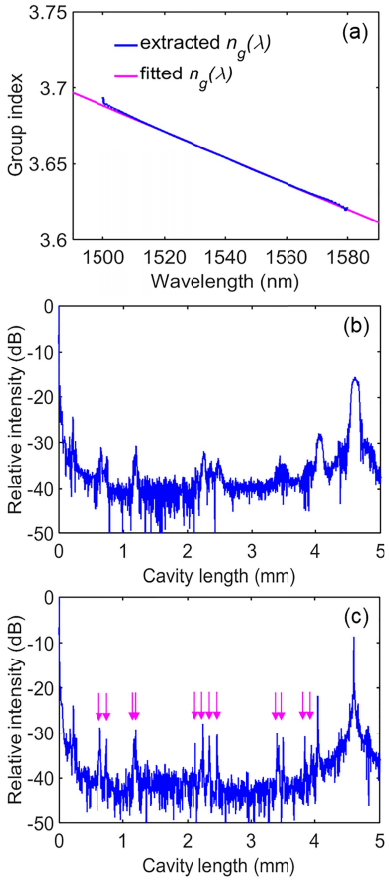

Fig. 4. (a) The wavelength dependent group index. The reflection distributions in spatial domain (b) before and (c) after de-embedding dispersion.

2.5 ± 0.5 dB/cm using the Fabry–Pérot interferometric method, the length of the chip L_{chip} is measured to be 4600 ± 15 μm. The RI at L_{chip} in Fig. 4(b) is -16 dB, which is significantly lower than the estimated value of -6.0 ± 0.6 dB. As shown in Fig. 4(c), the reflections peaks are narrower and sharper after de-embedding dispersion. The RI at L_{chip} is shown as -8 dB which is significantly improved, therefore it results in an enhanced accuracy of measurement. The tuning range of the laser source, the accuracy of the $n_g(\lambda)$ and $n_{\text{eff}}(\lambda)$, and the window functions could be still improved to further improve the peak accuracy. The positions of the peaks match accurately with the design values. We identify 12 reflection peaks at positions shown as magenta arrows instead of 16 peaks corresponding to 8 waveguide crossings due to overlap of the cavity lengths. The reflection at the cavity length of 4040 μm is visible in all measurements and is caused by a defect external to the device.

C. Positional Accuracy and Spatial Resolution

The reflections of the two crossings which are designed to be 30 μm apart can be resolved nicely as shown in Fig. 5(a). The measured distance d between the two reflection peaks is 28 μm, which is at least four times larger than the full width at half maximum (FWHM) of the two peaks, which are 7 μm and 4 μm, respectively. The results are based on a spline interpolation of the raw data.

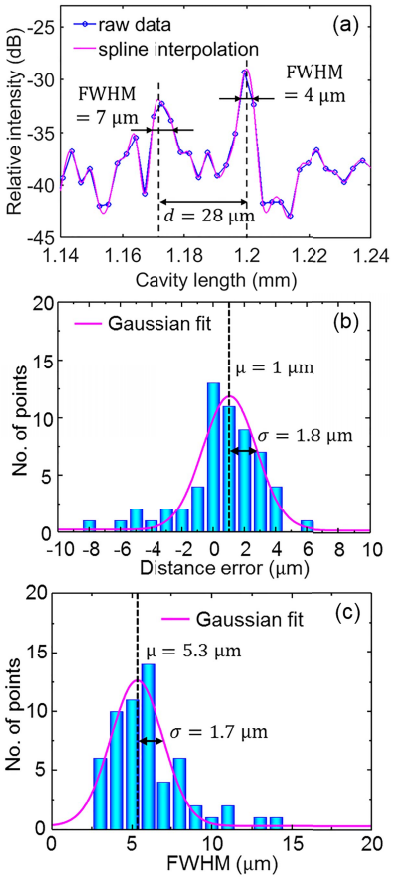

Fig. 5. (a) The reflections of two crossings with a design distance of 30 μm, (b) the distance error distribution and (c) the FWHM distribution of 58 measured peaks.

To confirm the positional accuracy of reflection peaks caused by crossings, we measured the distances d_{i1} between the i^{th} and the first reflection peaks caused by crossings in each sample. In this way, we remove the variations of the cleaving position of the facets. The distance error, $d_{i1} - d'_{i1}$, is the difference between the measured distance and the design value. A total number of 58 independent distance errors are measured and the distribution histogram is shown as Fig. 5(b). A fitted Gaussian curve of the error distribution is shown as the magenta line in Fig. 5(b), with a mean value μ of 1 μm and a standard deviation σ of 1.8 μm. Fig. 5(c) is the distribution histogram of FWHM of 58 measured peaks. A fitted Gaussian curve of the FWHM distribution is shown as the magenta line in Fig. 5(c), indicating a spatial resolution of 5.3 ± 1.7 μm.

D. Reflection of Waveguide Crossings

We use the results of RI after de-embedding dispersion to derive the reflection of crossings. The reflections of a total number of 58 crossings are analyzed. The reflection coefficient of the crossings can be calculated according to eq. (7) [7], [21] based on the same condition as eq. (6).

$$|r_{\text{c}}| \approx \frac{RI_{\text{c}}}{|r_{\text{f}}|\text{e}^{-\alpha z_{\text{c}}}} \tag{7}$$

where z_{c} is the actual position of the crossings, RI_{c} is the relative intensity at z_{c}. The power reflection $|r_{\text{c}}|^2$ of crossings is calculated to be $(2.5 \pm 1.2) \cdot 10^{-6}$.

IV. Conclusions

We presented a high-resolution OFDR method to measure localized reflections. The spatial resolution of the method was demonstrated to be 5.3 ± 1.7 μm. We used this method to characterize waveguide crossings. The reflection loss of a waveguide crossing was found to be $(2.5 \pm 1.2) \cdot 10^{-6}$.

References

[1] W. Bogaerts, M. Fiers, and P. Dumon, "Design challenges in silicon photonics," *IEEE J. Sel. Topics Quantum Electron.*, vol. 20, no. 4, pp. 1–8, Jul. 2014.
[2] E. Kleijn, D. Melati, A. Melloni, T. de Vries, M. Smit, and X. Leijtens, "Multimode interference couplers with reduced parasitic reflections," *IEEE Photon. Technol. Lett.*, vol. 26, no. 4, pp. 408–410, Feb. 15, 2014.
[3] P. Oberson, B. Huttner, O. Guinnard, L. Guinnard, G. Ribordy, and N. Gisin, "Optical frequency domain reflectometry with a narrow linewidth fiber laser," *IEEE Photon. Technol. Lett.*, vol. 12, no. 7, pp. 867–869, Jul. 2000.
[4] B. J. Soller, D. K. Gifford, M. S. Wolfe, and M. E. Froggatt, "High resolution optical frequency domain reflectometry for characterization of components and assemblies," *Opt. Exp.*, vol. 13, no. 2, pp. 666–674, Jan. 2005.
[5] J. P. Von Der Weid, R. Passy, G. Mussi, and N. Gisin, "On the characterization of optical fiber network components with optical frequency domain reflectometry," *J. Lightw. Technol.*, vol. 15, no. 7, pp. 1131–1141, Jul. 1997.
[6] U. Glombitza and E. Brinkmeyer, "Coherent frequency-domain reflectometry for characterization of single-mode integrated-optical waveguides," *J. Lightw. Technol.*, vol. 11, no. 8, pp. 1377–1384, Aug. 1993.
[7] A. Kohlhaas, C. Fröomchen, and E. Brinkmeyer, "High-resolution OCDR for testing integrated-optical waveguides: Dispersion-corrupted experimental data corrected by a numerical algorithm," *J. Lightw. Technol.*, vol. 9, no. 11, pp. 1493–1502, Nov. 1991.
[8] P. Beaud, J. Schutz, W. Hodel, H. P. Weber, H. H. Gilgen, and R. P. Salathe, "Optical reflectometry with micrometer resolution for the investigation of integrated optical devices," *IEEE J. Quantum Electron.*, vol. 25, no. 4, pp. 755–759, Apr. 1989.
[9] S.-H. Yun, G. J. Tearney, J. F. de Boer, N. Iftimia, and B. E. Bouma, "High-speed optical frequency-domain imaging," *Opt. Exp.*, vol. 11, no. 22, pp. 2953–2963, Nov. 2003.
[10] D. Melati, A. Alippi, and A. Melloni, "Waveguide-based technique for wafer-level measurement of phase and group effective refractive indices," *J. Lightw. Technol.*, vol. 34, no. 4, pp. 1293–1299, Feb. 15, 2016.
[11] K. Iizuka and S. Fujii, "A fault locator for integrated optics," in *Proc. 8th Opt. Fiber Sensors Conf.*, Jan. 1992, pp. 297–300.
[12] M. Smit *et al.*, "An introduction to InP-based generic integration technology," *Semicond. Sci. Technol.*, vol. 29, no. 8, p. 083001, 2014.
[13] D. Melati, "A design kit perspective is InP-based photonic integrated circuits," Ph.D. dissertation, Polytech. Univ. Milan, Milan, Italy, 2014.
[14] T.-J. Ahn and D. Kim, "High-resolution differential mode delay measurement for a multimode optical fiber using a modified optical frequency domain reflectometer," *Opt. Exp.*, vol. 13, no. 20, pp. 8256–8262, Oct. 2005.
[15] S. Morasca, F. Pozzi, and C. De Bernardi, "Measurement of group effective index in integrated semiconductor optical waveguides," *IEEE Photon. Technol. Lett.*, vol. 5, no. 1, pp. 40–42, Jan. 1993.
[16] S. Dwivedi *et al.*, "Experimental extraction of effective refractive index and thermo-optic coefficients of silicon-on-insulator waveguides using interferometers," *J. Lightw. Technol.*, vol. 33, no. 21, pp. 4471–4477, Nov. 1, 2015.
[17] J. Buus and M. Adams, "Phase and group indices for double heterostructure lasers," *IEEE J. Solid-State Electron Devices*, vol. 3, no. 6, pp. 189–195, Nov. 1979.
[18] R. B. Randall, *Frequency Analysis*, 3rd ed. Naerum, Denmark: Brüel & Kjaer, 1987.
[19] X. J. M. Leijtens, "JePPIX: the platform for InP-based photonics," *IET Optoelectron.*, vol. 5, no. 5, pp. 202–206, 2011. [Online]. Available: http://www.jeppix.eu
[20] F. Fiedler and A. Schlachetzki, "Optical parameters of InP-based waveguides," *Solid-State Electron.*, vol. 30, no. 1, pp. 73–83, 1987.
[21] W. Drexler and J. G. Fujimoto, *Optical Coherence Tomography: Technology and Applications*. Berlin, Germany: Springer, 2008.
[22] P.-A. Besse, J.-S. Gu, and H. Melchior, "Reflectivity minimization of semiconductor laser amplifiers with coated and angled facets considering two-dimensional beam profiles," *IEEE J. Quantum Electron.*, vol. 27, no. 6, pp. 1830–1836, Jun. 1991.